AIP | Review of Scientific Instruments

Analysis of a novel flexure hinge with three degrees of freedom

Feng-Zone Hsiao and Tai-Wu Lin

Citation: Review of Scientific Instruments **72**, 1565 (2001); doi: 10.1063/1.1340024
View online: http://dx.doi.org/10.1063/1.1340024
View Table of Contents: http://scitation.aip.org/content/aip/journal/rsi/72/2?ver=pdfcov
Published by the AIP Publishing

Articles you may be interested in

Design and testing of a novel multi-stroke micropositioning system with variable resolutions
Rev. Sci. Instrum. **85**, 025002 (2014); 10.1063/1.4866475

Design and implementation of a novel rotary micropositioning system driven by linear voice coil motor
Rev. Sci. Instrum. **84**, 055001 (2013); 10.1063/1.4803187

Development of a novel 3-degrees of freedom flexure based positioning system
Rev. Sci. Instrum. **83**, 055114 (2012); 10.1063/1.4720410

Design and control of a decoupled two degree of freedom translational parallel micro-positioning stage
Rev. Sci. Instrum. **83**, 045105 (2012); 10.1063/1.3700182

A six-degree-of-freedom precision motion stage
Rev. Sci. Instrum. **73**, 2462 (2002); 10.1063/1.1476717

JANIS
Does your research require low temperatures? Contact Janis today.
Our engineers will assist you in choosing the best system for your application.

10 mK to 800 K
LHe/LN$_2$ Cryostats
Cryocoolers
Magnet Systems
Dilution Refrigerator Systems
Micro-manipulated Probe Stations
sales@janis.com
www. janis.com
Click to view our product web page.

This article is copyrighted as indicated in the article. Reuse of AIP content is subject to the terms at: http://scitationnew.aip.org/termsconditions. Downloaded to IP: 140.113.38.11 On: Thu, 01 May 2014 07:19:41

Analysis of a novel flexure hinge with three degrees of freedom

Feng-Zone Hsiao[a)]
Synchrotron Radiation Research Center, No.1 R&D Road VI, Science-Based Industrial Park, Hsinchu 30077, Taiwan, Republic of China

Tai-Wu Lin
Department of Mechanical Engineering, National Chiao Tung University, Hsinchu, Taiwan, Republic of China

(Received 9 August 2000; accepted for publication 11 November 2000)

The flexure hinge is widely used as the mechanism for a high precision positioning stage with a micrometer or nanometer resolution. In this article we propose a novel flexure hinge with three degrees of freedom in which the motions are restricted in the same plane. An analysis model is developed to analyze the flexure hinge. The results obtained are consistent with those of the finite element method. A characteristic study using the proposed model shows that this flexure hinge has a feature of linear load displacement. In addition, the most effective way to change the stiffness of this flexure hinge is to modify the notch's radius. A prototype of this novel flexure hinge has been manufactured and the measured characteristics prove the advantages of this proposed model. © *2001 American Institute of Physics.* [DOI: 10.1063/1.1340024]

I. INTRODUCTION

The need for micromotion stage has found wide application in fields like the lithography process of the semiconductor industry, optical device tuning, ultraprecision machining, analysis of material surface structure, and the direct manipulation of DNA in genetic engineering. Nowadays, trends of miniaturization push the resolution of stage toward to the scale of nanometer or even subnanometer. Stages with high precision using sliding and rolling bearings of various types are inherently subjected to stick-slip and backlash problems for small displacement. The flexure hinge is a way to avoid such problems. It can be used to smoothly transfer the motion provided by actuators with sufficient resolution.

In fine stage design the flexure hinges with one or two axes of motion are usually used in which the fine motion is achieved either directly using the flexure hinge to transfer the small displacement from actuators like piezoelectric ones[1,2] or using the flexure hinge magnification mechanism to obtain a larger stroke.[3,4] In those applications the flexure hinge is usually the notch type which is formed through the machining of the high precision numerical controlled cutting machine. Because of the advancement of manufacturing technology, the profiles of notch-type flexure hinges can have right-circular, corner-filleted, and elliptical forms.[5] The notch-type flexure hinge usually has one axis of motion. Flexure hinges with two axes of motion can be formed either from the universal joint with coincident axes or by combining two notch-type hinges with perpendicular rotation axes together. For the study of flexure hinges Paros and Weisbord[6] presented an analysis formulation for evaluating the compliance of the notch-type flexure hinges with right-circular profiles and then investigated the characteristics of such kinds of flexure hinges. The limitation used in their analysis is that the minimum hinge thickness is much smaller than both the cutting notch radius and the hinge height. Smith, Chetwynd, and Bowen[7] showed an approximate formula, which was derived from the finite element analysis result, to evaluate the compliance of right-circular profile hinges for cases of larger minimum hinge thickness. The analysis formulations for the flexure hinges with elliptical profiles were presented by Smith *et al.*[8] Xu and King[5] compared the performance of different flexure hinge profiles by the finite element method (FEM) and they concluded that the flexure hinge with elliptical profiles has a lower maximum stress and thus a long fatigue life while the corner-filleted profiles offer the highest flexibility.

In this article we propose a novel monolithic flexure hinge with three degrees of freedom, where motions in the same plane with two translation and one rotation are allowed. An analytical model is proposed for the analysis and design of the flexure hinge and the finite element method is used to compare the results obtained from this model. The characteristics of the flexure hinge are then studied. Based on this study, a prototype is manufactured and its characteristics are measured to verify the results from the analysis model.

II. CONFIGURATION

Figure 1 shows the geometric configuration of the novel flexure hinge, where two notches with radius ρ_1 and ρ_2 are located, respectively, at the left and top region and two concentric arcs form the boundary of the corner region. The width of the horizontal and vertical straight section can be different and the thickness of the flexure hinge is uniform. The central points of the arcs at the left end notch generally have an offset with the edge of the adjacent straight section. A similar condition holds for the notch at the top end. The span angle of the outer arc (radius R_0) in the corner region is 90° and the two ends of this arc are tangent to the edges of

a)Electronic mail: fzh@srrc.gov.tw

 © 2001 American Institute of Physics
This article is copyrighted as indicated in the article. Reuse of AIP content is subject to the terms at: http://scitationnew.aip.org/termsconditions. Downloaded to IP: 140.113.38.11 On: Thu, 01 May 2014 07:19:41

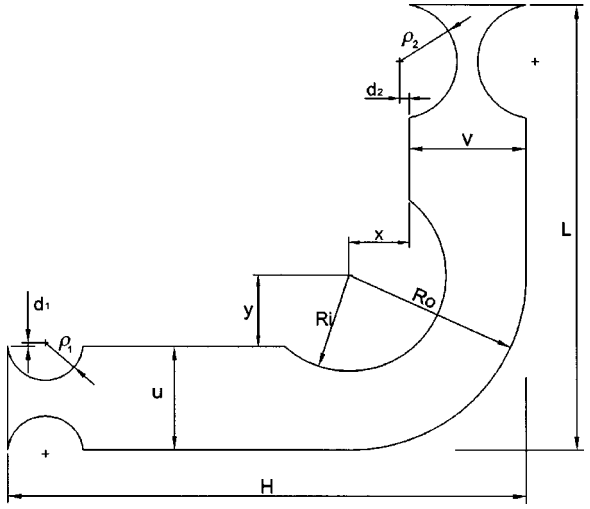

FIG. 1. General geometry of the flexure hinge.

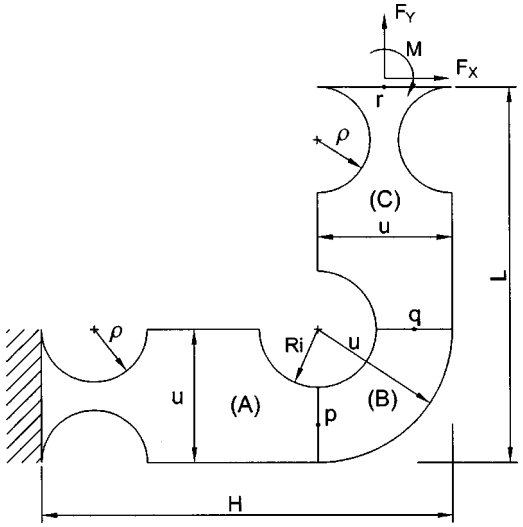

FIG. 3. Simplified model.

their adjacent straight sections, respectively. If the left-hand side of the flexure hinge is clamped and the forces and moment are applied at the top end, the flexure hinge will move in horizontal, vertical, and rotational directions. That is, the flexure hinge has three degrees of freedom in the same motion plane. A monolithic stage using this type of flexure hinge is shown in Fig. 2, where four flexure hinges placed at the corners of the stage are oriented to form a symmetric structure. Due to the unique feature of the flexure hinge, this stage has 3 motional degrees of freedom.

III. ANALYSIS MODEL

Figure 3 shows the simplified model of the flexure hinge. In this model the offset is set to zero and the notch radius at the left and top ends is set to the same value. The central point of the two concentric arcs at the corner is set as the intersection of the two extension lines from the edges of the horizontal and vertical straight sections. That is, the span angle of the inner arc is 270°. Though we simplify the geometric configuration, the following analysis procedure can still be applied to the general configuration.

In Fig. 3 the flexure hinge is divided into three segments A, B, and C. Segments A and C are treated as beam and the one-dimensional beam theory model is used to evaluate the deformation of each section. The left end is clamped and thus both the translation and rotation degrees of freedom are constrained. At the top end position the external force F_X, F_Y, M are applied here and this position is also regarded as the output point. The deflection curve for the neutral axis of the flexure hinge at segments A and C can be expressed by the differential equation

$$EI(x)\frac{d^2y}{dx^2}=M(x), \tag{1}$$

where the notations x and y are defined in Fig. 4, E is the Young's modulus, I is the cross sectional area moment of inertia of the neutral axis, and $M(x)$ is the bending moment at the given point x, which can be expressed as follows:

$$M(x)=M+F_Y(H-0.5u)-F_X(L-0.5u)-F_Yx. \tag{2}$$

The assumptions used in Eq. (1) are small deflection, small rotation and $d^2y/dx^2 \ll 1$.[9] Since the thickness of the flexure hinge is uniform, $I(x)$ at the straight section is a constant value. At the notch region $I(x)$ can be expressed as

$$I(x)=2bh^3(x)/3, \tag{3}$$

where b is the thickness of the flexure hinge and h is the half width of the notch region. The half width h at a given position x is expressed as

$$h(x)=0.5u-\sqrt{\rho^2-(\rho-x)^2}. \tag{4}$$

Thus the lateral deflection of the beam can be obtained from the integration of Eq. (1) and we have the following expressions:

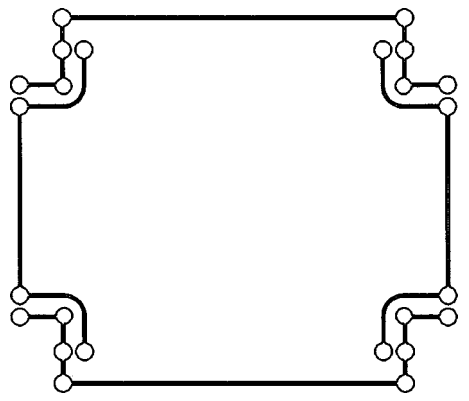

FIG. 2. A stage using the new flexure hinge.

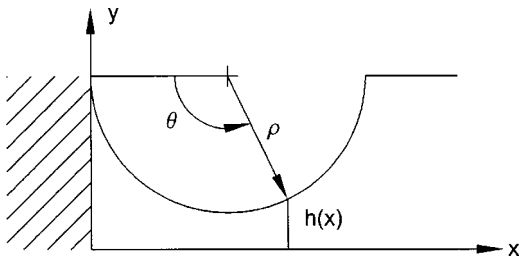

FIG. 4. Coordinate definition.

This article is copyrighted as indicated in the article. Reuse of AIP content is subject to the terms at: http://scitationnew.aip.org/termsconditions. Downloaded to IP: 140.113.38.11 On: Thu, 01 May 2014 07:19:41

At left notch region: $0 \leqslant x \leqslant 2\rho$ $(0 \leqslant \theta \leqslant \pi)$

$$
\begin{aligned}
y'(\theta) &= (c_1 - c_2\rho)\rho T[u,2\rho,\theta] + c_2\rho^2 P[u,2\rho,\theta] + A_1, \\
y(\theta) &= (c_1 - c_2\rho)\rho^2 Q[u,2\rho,\theta] + c_2\rho^3 S[u,2\rho,\theta] \\
&\quad + A_1(\rho - \rho\cos\theta) + A_2.
\end{aligned} \tag{5}
$$

At the horizontal straight section: $2\rho \leqslant x \leqslant H - u - R_i$

$$
\begin{aligned}
y'(x) &= \frac{c_1}{u^3}x - \frac{c_2}{2u^3}x^2 + A_3, \\
y(x) &= \frac{c_1}{2u^3}x^2 - \frac{c_2}{6u^3}x^3 + A_3 x + A_4.
\end{aligned} \tag{6}
$$

At notch adjacent to the corner region: $H\text{-}u\text{-}R_i \leqslant x \leqslant H - u$ $(0 \leqslant \theta \leqslant \pi/2)$

$$
\begin{aligned}
y'(\theta) &= (c_3 - c_2 R_i)R_i T[u,R_i,\theta] + c_2 R_i^2 P[u,R_i,\theta] \\
&\quad + c_4 R_i F[u,R_i,\theta] + A_5, \\
y(\theta) &= (c_3 - c_2 R_i)R_i^2 Q[u,R_i,\theta] + c_2 R_i^3 S[u,R_i,\theta] \\
&\quad + c_4 R_i^2 G[u,R_i,\theta] + A_5(R_i - R_i\cos\theta) + A_6.
\end{aligned} \tag{7}
$$

Here the integral functions $T[\cdot]$, $P[\cdot]$, $F[\cdot]$, $Q[\cdot]$, $S[\cdot]$, $G[\cdot]$, coefficients $c_1 \sim c_4$ and $A_1 \sim A_6$ are defined in the Appendix. In deriving Eqs. (5) and (7) we use the coordinate transformation in which the polar coordinate with origin at the center point of the arc boundary is used (see Fig. 4). Each term in Eqs. (5)–(7) can be expressed explicitly, though they are lengthy expressions. Thus we have the deformation formula expressed explicitly as a function of x at a given geometry and loading condition.

The axial displacement can be obtained by using the stress–strain relations for a beam subjected to the uniaxial load F:

$$
\begin{aligned}
\sigma_x &= \frac{F}{A}, \\
\varepsilon_x &= \frac{\sigma_x}{E}, \\
\Delta_x &= \int \varepsilon_x dx.
\end{aligned} \tag{8}
$$

Thus from Eqs. (7) and (8) the deformation at the interface between segment A and B (point p) can be obtained as follows:

$$
\begin{aligned}
X_p &= \frac{F_X}{Eb}\left(\rho W[u,2\rho,\pi] - \rho W[u,2\rho,0] + R_i W\left[u,R_i,\frac{\pi}{2}\right]\right. \\
&\quad \left. - R_i W[u,R_i,0] + \frac{H-u-R_i-2\rho}{u}\right), \\
Y_p &= (c_3 - c_2 R_i)R_i^2 Q\left[u,R_i,\frac{\pi}{2}\right] + c_2 R_i^3 S\left[u,R_i,\frac{\pi}{2}\right] \\
&\quad + c_4 R_i^2 G\left[u,R_i,\frac{\pi}{2}\right] + A_5 R_i + A_6,
\end{aligned} \tag{9}
$$

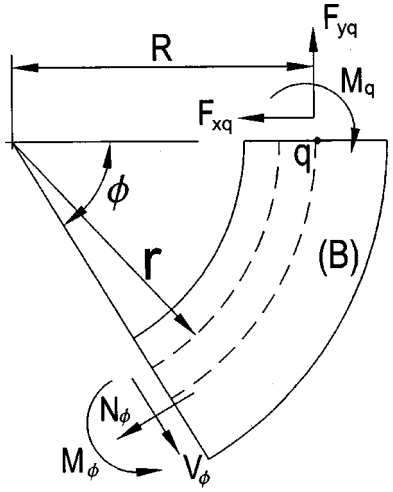

FIG. 5. Loading at Sec. B.

$$
\begin{aligned}
\theta_p &= (c_3 - c_2 R_i)R_i T\left[u,R_i,\frac{\pi}{2}\right] + c_2 R_i^2 P\left[u,R_i,\frac{\pi}{2}\right] \\
&\quad + c_4 R_i F\left[u,R_i,\frac{\pi}{2}\right] + A_5.
\end{aligned}
$$

In segment B, the energy method is used to obtain the displacement formula. Assume the plane section remains plane after loading and the contribution to strain energy from radial stress σ_r and out of plane stress σ_z are negligible compared with the contribution of circumferential stress σ_ϕ. The energy function U^* is then expressed as

$$
U^* = \int\int \left(\frac{\sigma_\phi^2}{2E} + \frac{\tau^2}{2G}\right) r\,d\phi\,dA. \tag{10}
$$

Since segment B is bounded by two concentric arcs it is a curved beam. The stress for a curved beam under the loading shown in Fig. 5 is expressed as[10]

$$
\begin{aligned}
\sigma_\phi &= \frac{M_\phi}{eA}\left(\frac{r_n}{r} - 1\right) + \frac{N_\phi}{A}, \\
\tau &= 1.2\,\frac{V_\phi^2}{A^2},
\end{aligned} \tag{11}
$$

where A is the cross sectional area and e and r_n are defined as below

$$
\begin{aligned}
r_n &= \frac{A}{\int \frac{dA}{r}} = \frac{u - R_i}{\ln(u) - \ln(R_i)}, \\
e &= R - r_n = \int \frac{r\,dA}{A} - r_n.
\end{aligned} \tag{12}
$$

From the free body diagram the force equilibrium condition shown in Fig. 5 can be expressed as

$$
\begin{aligned}
M_\phi &= M_q - F_{xq}R\cdot\sin\phi - F_{yq}R(1-\cos\phi), \\
N_\phi &= -F_{xq}\sin\phi + F_{yq}\cos\phi, \\
V_\phi &= F_{xq}\cos\phi + F_{yq}\sin\phi, \quad 0 \leqslant \phi \leqslant \frac{\pi}{2}
\end{aligned} \tag{13}
$$

This article is copyrighted as indicated in the article. Reuse of AIP content is subject to the terms at: http://scitationnew.aip.org/termsconditions. Downloaded to IP: 140.113.38.11 On: Thu, 01 May 2014 07:19:41

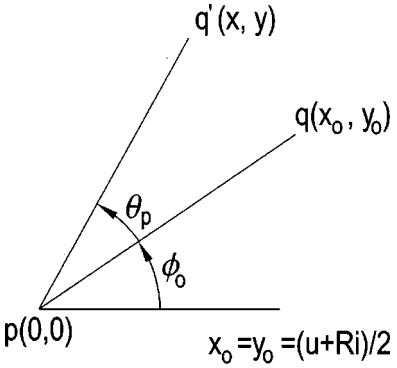

FIG. 6. Finite rotation.

where M_q, F_{xq}, and F_{yq} are the loadings at point q, which are related to the external loads by the following expressions:

$$\begin{aligned} M_q &= -M + F_X(L-u) + \tfrac{1}{2}F_Y R_i, \\ F_{\mathrm{xq}} &= -F_X, \\ F_{yq} &= F_Y. \end{aligned} \tag{14}$$

Based on the assumption of small displacement and linear elastic material, the deflection at point q can be expressed from Castigliano's theorem

$$\begin{aligned} \Delta_H &= \frac{\partial U^*}{\partial F_{xq}} = \frac{1}{EA}\left(1-\frac{R}{e}\right)\left(M_q + \frac{\pi R}{4}F_X - \frac{R}{2}F_Y\right) \\ &\quad + \frac{1.2R}{GA}\left(-\frac{\pi}{4}F_X + \frac{1}{2}F_Y\right), \\ \Delta_V &= \frac{\partial U^*}{\partial F_{yq}} = \frac{M_q}{EA}\left(\frac{R}{e}\left(1-\frac{\pi}{2}\right)-1\right) - \frac{F_X}{2EA}\left(\frac{R^2}{e} - R + \frac{1.2RE}{G}\right) \\ &\quad + \frac{F_Y}{EA}\left(\frac{R^2}{e}\left(\frac{3\pi}{4}-2\right) + R\left(2-\frac{\pi}{4}\right) + \frac{1.2\pi}{4}\frac{RE}{G}\right), \end{aligned} \tag{15}$$

$$\begin{aligned} \Delta_\theta &= \frac{\partial U^*}{\partial M_q} = \frac{1}{EAe}\left(\frac{\pi}{2}M_q + R\times F_X + R\times F_Y\left(1-\frac{\pi}{2}\right)\right) \\ &\quad - \frac{1}{EA}(F_X + F_Y). \end{aligned}$$

In addition to the deformation caused by the loading at point q, the displacement at q actually includes the finite rotation at point p as Fig. 6 shows. Neglecting the second order term and treating segment B as a rigid body one, the corresponding displacement Δx, Δy from the finite rotation is expressed as below

$$\begin{aligned} \Delta x &= x - x_0 = x_0(\cos\theta_p - 1) - y_0 \sin\theta_p, \\ \Delta y &= y - y_0 = x_0 \sin\theta_p + y_0(\cos\theta_p - 1). \end{aligned} \tag{16}$$

Thus the displacement at point q can be obtained as follows:

$$\begin{aligned} X_q &= X_p - \Delta_H + \frac{u+R_i}{2}\times(\cos\theta_p - \sin\theta_p - 1), \\ Y_q &= Y_p + \Delta_V + \frac{u+R_i}{2}\times(\sin\theta_p + \cos\theta_p - 1), \\ \theta_q &= \theta_p - \Delta_\theta. \end{aligned} \tag{17}$$

Deformation of segment C can be obtained through the same procedure as that in segment A. Continuous conditions in both displacement and slope are applied at the junction of segments B and C. With the local coordinate transformation $\eta = -x$ and $\xi = y$, the expressions for the lateral deflection at segment C can be obtained as follows:

At the notch region adjacent to the corner region

$$\begin{aligned} \eta'(\theta) &= c_5 R_i T[u,R_i,\theta] + 2c_4 R_i^2 P[u,R_i,\theta] \\ &\quad + \frac{c_2}{2}R_i F[u,R_i,\theta] + A_7, \\ \eta(\theta) &= c_5 R_i^2 Q[u,R_i,\theta] + 2c_4 R_i^3 S[u,R_i,\theta] \\ &\quad + \frac{c_2}{2}R_i^2 G[u,R_i,\theta] + A_7 R_i \cos\theta + A_8. \end{aligned} \tag{18}$$

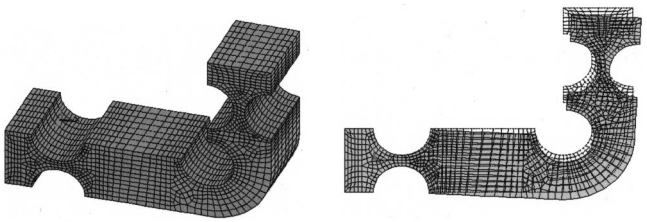

FIG. 7. Meshes and deformation.

TABLE I. Simulation results using both the analysis model and the finite element method.

Case			$Dx(\mu m)$			$Dy(\mu m)$			θz(mrad)	
Geometry	Loading	FEM	Analysis	Error (%)	FEM	Analysis	Error (%)	FEM	Analysis	Error (%)
A	A	259.67	265.02	−2.06	−350.72	−364.04	−3.80	−10.39	−10.02	3.55
B	A	286.54	292.42	−2.05	−398.81	−412.42	−3.41	−10.98	−10.94	0.42
A	B	217.10	212.39	2.17	−249.96	−260.15	−4.08	−9.84	−9.16	6.88
A	C	−51.08	−49.59	2.90	49.85	54.10	−8.52	2.91	3.04	−4.69
A	D	425.79	427.42	−0.38	−550.83	−570.47	−3.57	−17.08	−16.14	5.50

Remark:
Geometry A:ρ=5, Ri=5, u=12, H=45, L=30, b=16 mm.
Geometry B: ρ=4.8, Ri=5.2, u=11.6, H=46, L=30, b=15 mm.
Loading A: Fy=−60 N, Fx=M=0; Loading C: Fx=Fy=0, M=300 N mm.
Loading B: Fx=60 N, Fy=M=0; Loading D: Fx=60, Fy=−60 N, M=300 N mm.

This article is copyrighted as indicated in the article. Reuse of AIP content is subject to the terms at: http://scitationnew.aip.org/termsconditions. Downloaded to IP: 140.113.38.11 On: Thu, 01 May 2014 07:19:41

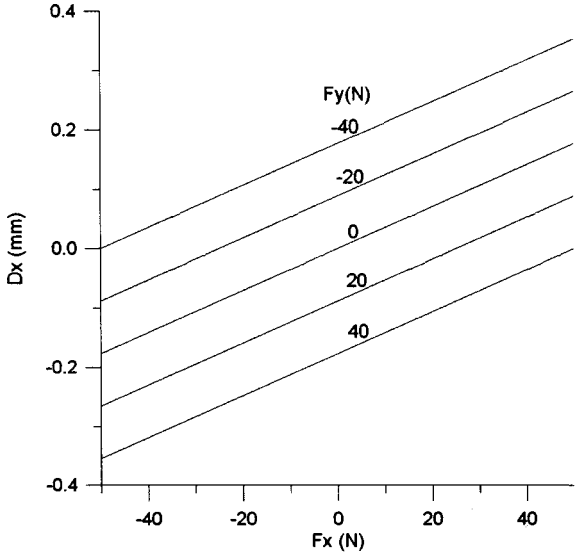

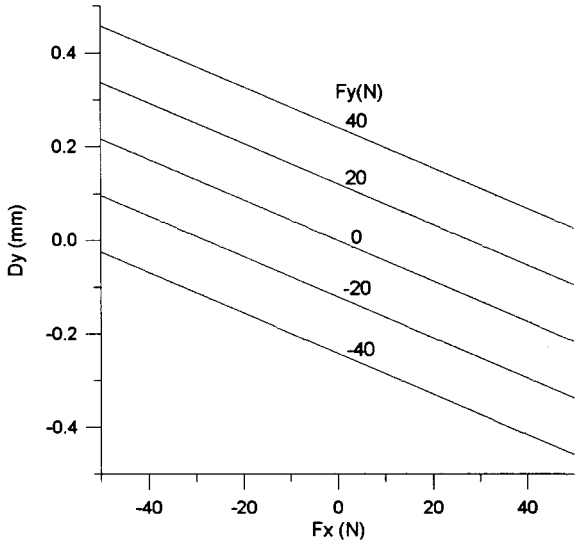

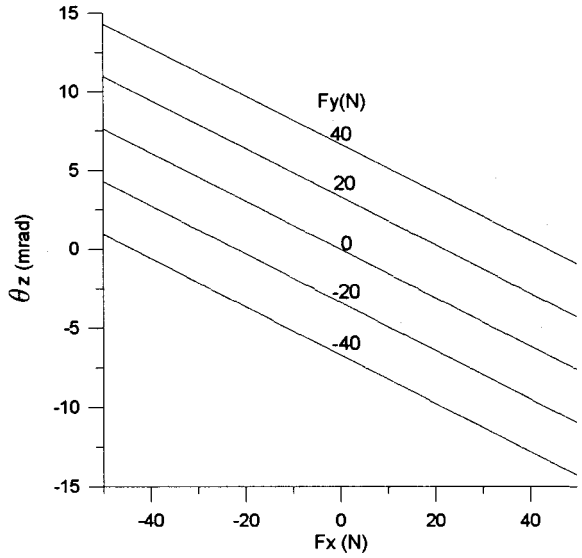

FIG. 8. Deformation at different F_X and F_Y.

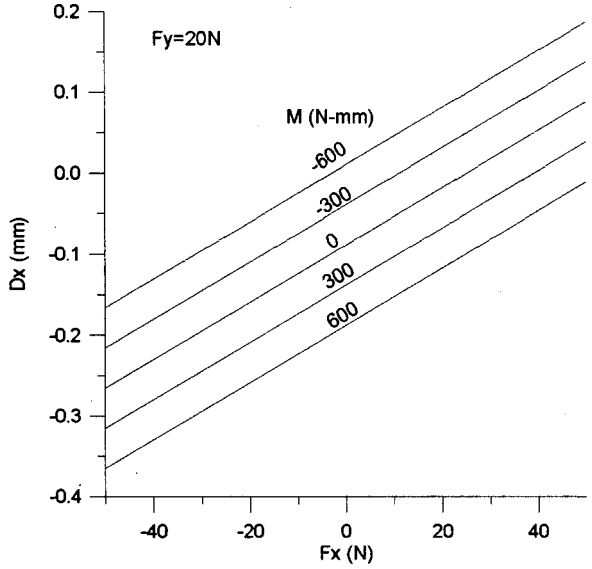

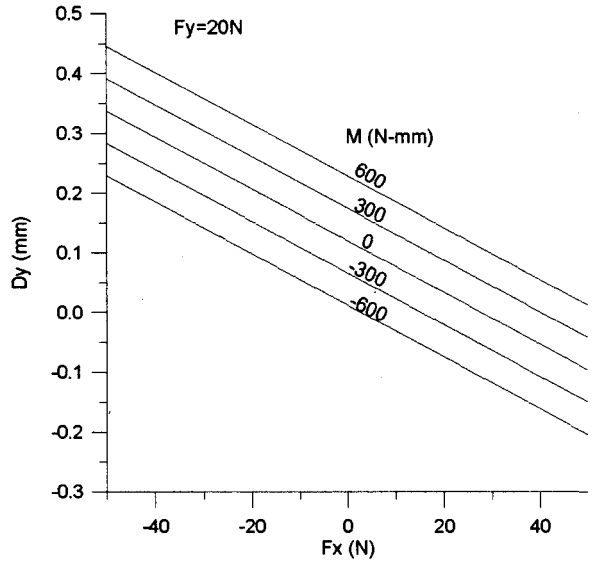

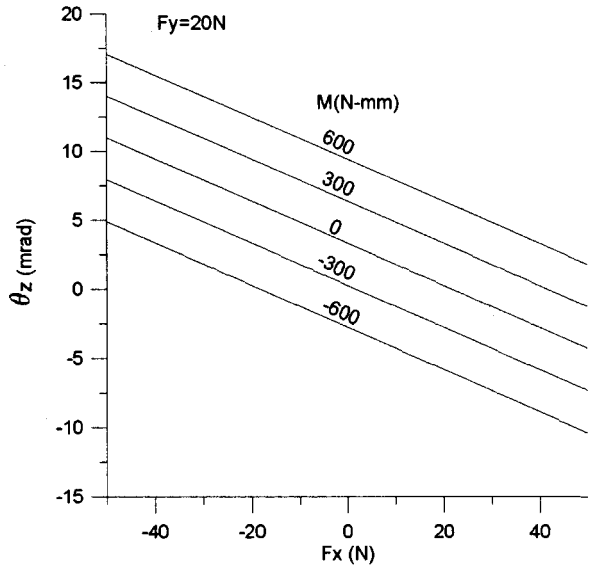

FIG. 9. Deformation at different moment M.

This article is copyrighted as indicated in the article. Reuse of AIP content is subject to the terms at: http://scitationnew.aip.org/termsconditions. Downloaded to IP: 140.113.38.11 On: Thu, 01 May 2014 07:19:41

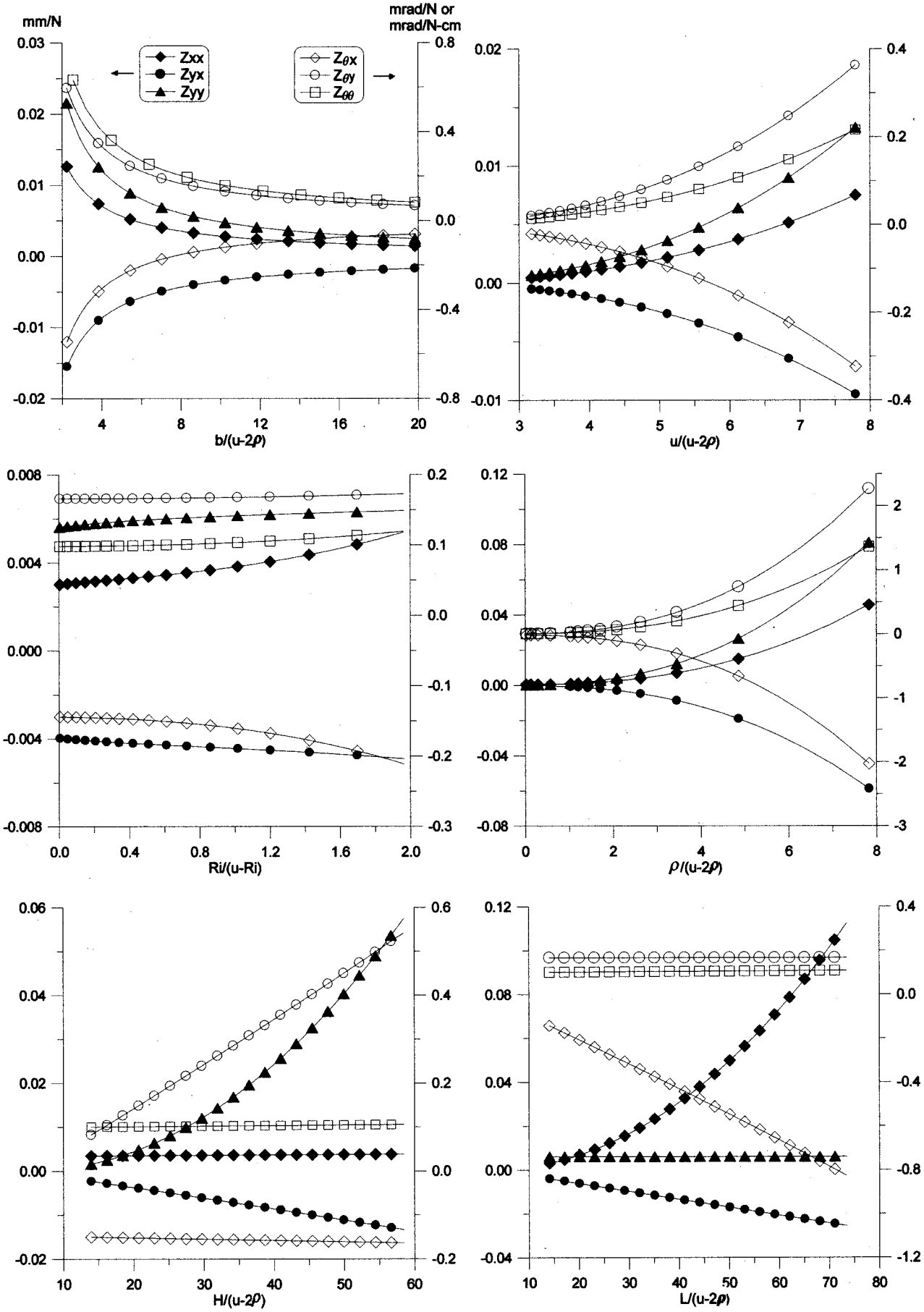

FIG. 10. Effect of geometry dimension on flexure compliance; $F_X = M = 0$, $F_Y = 20$ N.

This article is copyrighted as indicated in the article. Reuse of AIP content is subject to the terms at: http://scitationnew.aip.org/termsconditions. Downloaded to IP: 140.113.38.11 On: Thu, 01 May 2014 07:19:41

At the vertical straight section

$$\eta'(\xi)=c_6\xi+\frac{c_7}{2}\xi^2+A_9,$$
$$\eta(\xi)=\frac{c_6}{2}\xi^2+\frac{c_7}{6}\xi^3+A_9\xi+A_{10}. \tag{19}$$

At the top notch region

$$\eta'(\theta)=(c_8+2c_4\rho)\rho T[u,2\rho,\theta]-2c_4\rho^2P[u,2\rho,\theta]+A_{11},$$
$$\eta(\theta)=(c_8+2c_4\rho)\rho^2Q[u,2\rho,\theta]-2c_4\rho^3S[u,2\rho,\theta]+A_{11}(\rho-\rho\cos\theta)+A_{12}. \tag{20}$$

The axial displacement can be obtained by using Eq. (8). Thus the formulations for the displacement of the flexure hinge subjected to external loads at output point r can be obtained from Eqs. (8) and (20) and listed as below

$$X_r=-(c_8+2c_4\rho)\rho^2Q[u,2\rho,\pi]+2c_4\rho^3S[u,2\rho,\pi]-2\rho A_{11}-A_{12},$$
$$Y_r=Y_q+\frac{F_Y}{Eb}\left(R_iW\left[u,R_i,\frac{\pi}{2}\right]-R_iW[u,R_i,0]+\rho W[u,2\rho,\pi]-\rho W[u,2\rho,0]+\frac{L-R_i-u-2\rho}{u}\right), \tag{21}$$
$$\theta_r=(c_8+2c_4\rho)\rho T[u,2\rho,\pi]-2c_4\rho^2P[u,2\rho,\pi]+A_{11}.$$

Each term in Eq. (21) can be expanded in terms of either loading or geometric dimension and the explicit form is expressed in the Appendix.

IV. FINITE ELEMENT METHOD (FEM)

The motion of the flexure hinge is simulated by using the commercial FEM package ANSYS. Figure 7 shows the meshes used to analyze the flexure hinge. An eight-node element SOLID73, with 6 motional degrees of freedom (three translation and three rotation) on each node, is used to define the geometry and simulate the deformation. Since there are singularity problems at the left and top ends of the flexure hinge, the range of the geometric model at both ends is extended to avoid the mesh singularity. The clamped boundary condition is applied at the left-extended region. To reduce the effect of large stress gradient around the loaded region (Saint-Venant's principle), the loading is applied at the end of the top extended region. However, because of the extension at the top end, application of the horizontal force will give an additional moment at the notch end. A correction moment should be added in FEM analysis for cases of horizontal loading. Table I shows the simulation result obtained from both the analysis model and the finite element method, where the additional moment caused from horizontal load is compensated in FEM analysis. The enlarged scale of the typical deformation for the flexure hinge at a given loading is displayed in Fig. 7.

In Table I five different cases formed from two geometry and three external forces are analyzed. From different cases of comparison, both methods give a consistent result. The result shows smaller difference for cases of pure vertical loading and larger difference for cases of either horizontal force or moment loading exists. The maximum deviation here is 8.5%. A further study shows that the tolerance between the analysis result and FEM simulation is within 13% in case of $14<H/(u-2\rho)<58$, $14<L/(u-2\rho)<73$, $0.1<R_i/(u-R_i)<1.67$, $0.25<b/(u-2\rho)<20$, or $3.2<u/(u-2\rho)<7.67$. The tolerance is within 16% if $1<\rho/(u-2\rho)<4.5$.

V. CHARACTERISTICS

Using the analysis model we study the characteristic of the monolithic flexure hinge. Figure 8 shows the flexure hinge behavior for cases of different external horizontal loading F_X and vertical loading F_Y. The effect of adding external moment M is shown in Fig. 9. From Figs. 8 and 9 a linear relation between loading and displacement exits in all x, y, and θ_z directions. Furthermore, if one applies only either the horizontal force, the vertical force, or the pure moment at the top end, the flexure hinge will have the horizontal motion, the vertical motion, and the rotating motion simultaneously. That is, the flexure hinge has a coupled motion behavior. Since a linear relationship holds between the loading and the motion it is easy to compensate this coupled motion problem. From the linear relationship and coupled behavior the motion at the end point of the flexure hinge subject to external loading can be expressed as follows:

$$D_x=Z_{xx}F_X+Z_{xy}F_Y+Z_{x\theta}M,$$
$$D_y=Z_{yx}F_X+Z_{yy}F_Y+Z_{y\theta}M, \tag{22}$$
$$\theta_z=Z_{\theta x}F_X+Z_{\theta y}F_Y+Z_{\theta\theta}M.$$

Here Z_{IJ} represents the I-direction compliance due to J-direction loading.

Case studies for the effect of geometry dimension on the flexure characteristics for the same loading condition are shown in Fig. 10, where the constraint $u>R_i$, $u>2\rho$, $H>u+2\rho+R_i$, and $L>u+2\rho+R_i$ are applied. Only six curves are shown here because the compliances Z_{IJ} and Z_{JI}

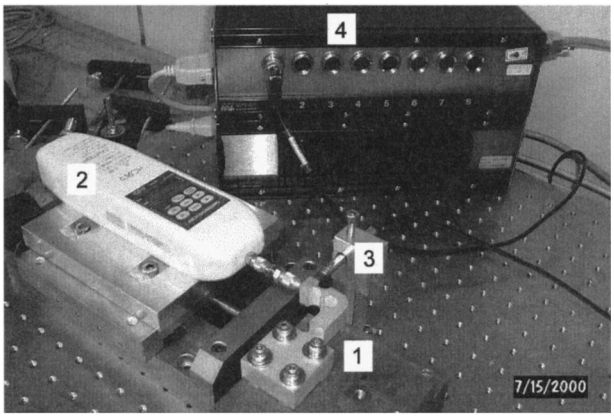

1 flexure hinge
2 force gauge
3 LVDT probe
4 probe signal processor

FIG. 11. Performance measurement of the prototype.

This article is copyrighted as indicated in the article. Reuse of AIP content is subject to the terms at: http://scitationnew.aip.org/termsconditions. Downloaded to IP: 140.113.38.11 On: Thu, 01 May 2014 07:19:41

TABLE II. Characteristics of the flexure prototype.

	Dx			Dy				Dx			Dy		
F_x (*Kgw*)	Measure (μm)	Analysis (μm)	Error (%)	Measure (μm)	Analysis (μm)	Error (%)	F_Y (*Kgw*)	Measure (μm)	Analysis (μm)	Error (%)	Measure (μm)	Analysis (μm)	Error (%)
1	38.6	34.7	−10.1	−42.6	−42.5	−0.2	1	−42.4	−43.4	2.4	72.5	59.3	−18.2
2	78.3	69.3	−11.5	−85.2	−85.1	−0.1	2	−82.5	−86.9	5.3	142.1	118.5	−16.6
3	118.6	104.0	−12.3	−126.9	−127.6	0.6	3	−118.5	−130.4	10.0	208.5	177.7	−14.8
4	158.8	138.6	−12.7	−168.3	−170.2	1.1	4	−153.4	−173.8	13.3	275.3	236.9	−13.9
5	200.6	173.2	−13.7	−210.9	−212.7	0.9	5	−188.3	−217.4	15.5	339.3	296.1	−12.7
6	240.7	207.8	−13.7	−254	−255.3	0.5	6	−223.7	−260.9	16.6	401.7	355.2	−11.6
−1	−37.2	−34.7	−6.7	38.5	42.5	10.4	−1	35.4	43.4	22.6	−57.4	−59.3	3.3
−2	−74.1	−69.4	−6.3	79.7	85.0	6.6	−2	73.1	86.8	18.7	−115.2	−118.6	3.0
−3	−111	−104.1	−6.2	122	127.5	4.5	−3	111.6	130.1	16.6	−179.9	−177.9	−1.1
−4	−146	−138.8	−4.9	161	170.0	5.6	−4	149.5	173.5	16.1	−238.1	−237.3	−0.3
−5	−177.4	−173.5	−2.2	195.3	212.4	8.8	−5	190.2	216.8	14.0	−298.5	−296.6	−0.6
−6	−204	−208.2	2.1	222.8	254.9	14.4	−6	223.6	260.1	16.3	−360.8	−356.0	−1.3

have similar value. From Fig. 10 all the compliances show strong sensitivity to the change of the notch's cutting radius ρ, flexure thickness b, and width u, where the most sensitive factor is ρ. Changing the corner radius R_i has not as apparent an effect as ρ does. Changing the magnitude of H has a strong effect on the compliances Z_{yy}, Z_{yx}, and $Z_{\theta y}$; similar conditions hold for the case of changing L except that the directions x and y are interchanged.

A prototype is fabricated to check the accuracy of the analysis model. The loading in either horizontal or vertical direction is applied to test the characteristics of this flexure prototype. Figure 11 shows the measurement setup of this prototype. A force gauge is used to measure the magnitude of the applied loads. Deformation of the prototype is measured through the 0.1 μm accuracy linear variable differential transformer probe. Table II shows the measured result for different loading conditions; the results estimated from the analysis model are also shown here for comparison. From Table II the analysis model provides a good estimation in the case of horizontal loading and a less accurate estimation in the case of vertical loading. The measured result also proves the linear load-displacement feature of the flexure hinge.

ACKNOWLEDGMENTS

This study was supported by the National Science Council, Republic of China, under Contract No. NSC88-2218-E-213-003.

APPENDIX

$$T[u,d,\theta]=\int \frac{\sin\theta}{(u-d\times\sin\theta)^3}d\theta,$$

$$P[u,d,\theta]=\int \frac{\sin\theta\times\cos\theta}{(u-d\times\sin\theta)^3}d\theta,$$

$$Q[u,d,\theta]=\int T[u,d,\theta]\times\sin\theta d\theta,$$

$$S[u,d,\theta]=\int P[u,d,\theta]\times\sin\theta d\theta,$$

$$F[u,d,\theta]=\int \frac{\sin\theta}{(u-d\times\sin\theta)^2}d\theta,$$

$$G[u,d,\theta]=\int F[u,d,\theta]\sin\theta d\theta,$$

$$W[u,d,\theta]=\int \frac{\sin\theta}{(u-d\times\sin\theta)}d\theta,$$

$$c_1=\frac{M+F_Y(H-u/2)-F_X(L-u/2)}{Eb/12},\quad c_2=\frac{F_Y}{Eb/12},$$

$$c_3=\frac{M+F_Y(R_i+u/2)-F_XL}{Eb/12},\quad c_4=\frac{F_X}{Eb/6},$$

$$c_5=\frac{M-F_X(L-u)-F_Yu/2}{Eb/12},\quad c_6=\frac{M-F_X(L-u-R_i)}{Ebu^3/12},$$

$$c_7=\frac{F_X}{Ebu^3/12},\quad c_8=\frac{M-2F_X\rho}{Eb/12},$$

$$A_1=-(c_1-c_2\rho)\rho T[u,2\rho,0]-c_2\rho^2P[u,2\rho,0],$$

$$A_2=-(c_1-c_2\rho)\rho^2Q[u,2\rho,0]-c_2\rho^3S[u,2\rho,0],$$

$$A_3=A_1-\frac{2c_1\rho-2c_2\rho^2}{u^3}+(c_1-c_2\rho)\rho T[u,2\rho,\pi]+c_2\rho^2P[u,2\rho,\pi],$$

$$A_4=A_2+2(A_1-A_3)\rho-\frac{2c_1\rho^2}{u^3}+\frac{4c_2\rho^3}{3u^3}+(c_1-c_2\rho)\rho^2Q[u,2\rho,\pi]+c_2\rho^3S[u,2\rho,\pi],$$

$$A_5=A_3+\frac{c_1}{u^3}(H-u-R_i)-\frac{c_2}{2u^3}(H-u-R_i)^2-(c_3-c_2R_i)R_iT[u,R_i,0]-c_2R_i^2P[u,R_i,0]-c_4R_iF[u,R_i,0],$$

This article is copyrighted as indicated in the article. Reuse of AIP content is subject to the terms at: http://scitationnew.aip.org/termsconditions. Downloaded to IP: 140.113.38.11 On: Thu, 01 May 2014 07:19:41

$$A_6=A_4+A_3(H-u-R_i)+\frac{c_1}{2u^3}(H-u-R_i)^2$$
$$-\frac{c_2}{6u^3}(H-u-R_i)^3$$
$$-(c_3-c_2R_i)R_i^2Q[u,R_i,0]-c_2R_i^3S[u,R_i,0]$$
$$-c_4R_i^2G[u,R_i,0],$$

$$A_7=\theta_q-c_5R_iT\left[u,R_i,\frac{\pi}{2}\right]-2c_4R_i^2P\left[u,R_i,\frac{\pi}{2}\right]$$
$$-\frac{c_2}{2}R_iF\left[u,R_i,\frac{\pi}{2}\right],$$

$$A_8=-X_q-c_5R_i^2Q\left[u,R_i,\frac{\pi}{2}\right]-2c_4R_i^3S\left[u,R_i,\frac{\pi}{2}\right]$$
$$-\frac{c_2}{2}R_i^2G\left[u,R_i,\frac{\pi}{2}\right],$$

$$A_9=A_7+c_5R_iT[u,R_i,0]+2c_4R_i^2P[u,R_i,0]$$
$$+\frac{c_2}{2}R_iF[u,R_i,0],$$

$$A_{10}=A_8+A_7R_i+c_5R_i^2Q[u,R_i,0]+2c_4R_i^3S[u,R_i,0]$$
$$+\frac{c_2}{2}R_i^2G[u,R_i,0],$$

$$A_{11}=A_9+c_6(L-u-R_i-2\rho)+\frac{c_7}{2}(L-u-R_i-2\rho)^2$$
$$-(c_8+2c_4\rho)\rho T[u,2\rho,0]+2c_4\rho^2P[u,2\rho,0],$$

$$A_{12}=A_{10}+A_9(L-u-R_i-2\rho)+\frac{c_6}{2}(L-u-R_i-2\rho)^2$$
$$+\frac{c_7}{6}(L-u-R_i-2\rho)^3$$
$$-(c_8+2c_4\rho)\rho^2Q[u,2\rho,0]+2c_4\rho^3S[u,2\rho,0].$$

[1] M. Taniguchi, M. Ikeda, A. Inagaki, and R. Funatsu, Int. J. Jpn. Soc. Precis. Eng. **26**, 35 (1992).
[2] M. R. Howells, Opt. Eng. (Bellingham) **34**, 410 (1995).
[3] F. E. Scire and E. C. Teague, Rev. Sci. Instrum. **49**, 1735 (1978).
[4] S. H. Chang and B. C. Du, Rev. Sci. Instrum. **69**, 1785 (1998).
[5] W. Xu and T. King, Precis. Eng. **19**, 4 (1997).
[6] J. M. Paros and L. Weisbord, Mach. Des. **37**, 151 (1965).
[7] S. T. Smith, D. G. Chetwynd, and D. K. Bowen, J. Phys. E **20**, 977 (1987).
[8] S. T. Smith, V. G. Badami, J. S. Dale, and Y. Xu, Rev. Sci. Instrum. **68**, 1474 (1997).
[9] J. M. Gere and S. P. Timoshenko, *Mechanics of Materials* (PWS Engineering, Boston, 1984), p. 354.
[10] R. D. Cook and W. C. Young, *Advanced Mechanics of Materials* (Macmillan, New York, 1985), p. 416.

This article is copyrighted as indicated in the article. Reuse of AIP content is subject to the terms at: http://scitationnew.aip.org/termsconditions. Downloaded to IP: 140.113.38.11 On: Thu, 01 May 2014 07:19:41